ACS PHYSICAL CHEMISTRY Au
AN OPEN ACCESS JOURNAL OF THE AMERICAN CHEMICAL SOCIETY

pubs.acs.org/physchemau
Article

Spinodal Decomposition by a Two-Step Procedure for Nano Porous Silica

Zuyi Zhang*

Cite This: ACS Phys. Chem Au 2024, 4, 696−706
Read Online

ABSTRACT: The phase separation of the $Na_2O-B_2O_3-SiO_2$ system was explored both theoretically and experimentally in order to attain a spinodal structure having a narrowed periodic distance (<70 nm) with the porosity being kept at ∼60%. The phase separation was dealt with by two stages: an initial thermodynamic process of spinodal decomposition and a latter growth of the spinodal structure. The initial structural development was related to the interfacial energy and the change in free energy caused by phase separation. For the latter growth, a mathematical model was proposed to explain the kinetics by incorporating the effect of the inverse-square law in the diffusion of SiO_2, and a basic relation of $d^3 - d_0^3 \propto t$ (d: average periodic distance; t: time) was successfully derived. The phase separation was carried out accordingly by two steps: first for the phase separation forming durable silica skeletons at lower temperatures and second for the new equilibrium at the elevated temperature and the subsequent growth of the phase-separated structure. It was proven that the addition of Al_2O_3 in the glasses decreased the interfacial energy, leading to small periodic distances and the rapid establishment of the durable silica skeletons. In the two-step process, the fraction of borate-rich phase increased, and the structure grew depending on a modified period of time.

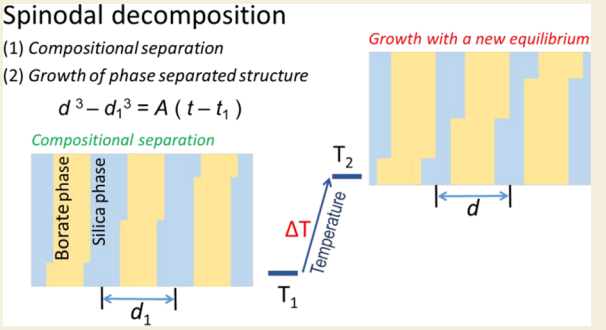

KEYWORDS: *spinodal decomposition, porous silica, two-step procedure, interfacial energy, periodic distance, porosity*

1. INTRODUCTION

It is well known that spinodal decomposition is one of the promising technologies to attain porous materials.[1−4] In the sodium borosilicate system,[2,5] when a metastable glass falls to the spinodal region with decreasing temperature, it can separate into SiO_2-rich phase and borate-rich phase via infinitesimal fluctuation of composition, which is ascribed to a negative $\partial^2 g(C)/\partial C^2$ [$g(C)$: free energy, C: concentration].[6] A porous silica can be obtained by selectively etching the borate-rich phase with acid. On the other hand, phase separation via sol−gel processes has been ascribed to polymerization-induced reduction in mutual solubility,[7] and then freezing with sol−gel transition.[8] The phase separation is ascribed to a decrease in free energy that may be caused either thermally or chemically. As to the dimension, the pore size of the porous silica derived from sol−gel processes ranged from 0.1 to several micrometers,[9] whereas that of the porous silica derived from borosilicate glasses ranged from 4 to 300 nm.[10]

Hierarchically porous materials were achieved by the sol−gel method for application of high-performance liquid chromatography.[11] However, we have been motivated by the sodium borosilicate system because of the low scattering of light in the visible region. A new type of antireflective coating was attained, in which the low refractive index was realized based on a high porosity of ∼60%,[12] dust proof was related to the width of SiO_2 skeletons,[13] and antifogging property was attributed to the pore size distribution.[14] A strong SiO_2 network consisting mainly of Q^4 units[15] was favored from the point of view of capillary force in an ambient atmosphere. On the other hand, the thickness of the coating reached several micrometers, which was considerably thick compared with the normal optical films.[16−18] Ogawa and Nakamura treated the scattering of light of Vycor silica on the basis of structural fluctuation,[19] and a relation of $I \sim d^3 l$ is considered to be applicable for an inhomogeneous coating (I: intensity of light scattering, d: average periodic distance of the structure, and l: thickness).[20] A structural region of spinodal silica having average periodic distances less than 70 nm and a high porosity of ∼60% is desired for the optical application of inhomogeneous coatings in order to accommodate the large thickness up to 5 μm. The porosity was determined in order to achieve the reflection as low as 0.5%,[12] and the average periodic distance was required to lower the light scattering to a degree of an optical coating based on SWS (subwavelength structure).[17]

Received: July 29, 2024
Revised: September 24, 2024
Accepted: September 25, 2024
Published: October 3, 2024

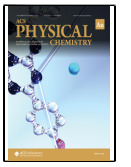

https://doi.org/10.1021/acsphyschemau.4c00060
ACS Phys. Chem Au 2024, 4, 696−706

In addition, a high porosity is always favored in a separation membrane unless other properties such as the mechanical strength become unaffordable.

To our knowledge, to obtain high porosity with favorable durability in the $Na_2O-B_2O_3-SiO_2$ system, the temperature for an equilibrium between the two phases should be as high as 600 °C, and porous glasses with periodic distances less than 100 nm are unavailable yet. In this study, the phase separation was dealt with theoretically by dividing into two stages, and a two-step procedure was proposed. The experimental conditions were designed to verify the effects of ΔG (the change of free energy) caused by a change of temperature and γ (the interfacial energy) by the fourth component as well as the kinetics of growth as a function of heat-treatment time. As to the experimental feature, the surfaces of glass samples were well-polished, and the top surfaces of the resultant porous glasses allowed the quantitative analysis of the spinodal decomposition (Supporting Information). The average periodic distance, d, was defined as the average distance between the middle points of adjacent silica skeletons, the average width of skeletons to that of silica skeletons having uppermost surfaces, and the porosity to the volume fraction of pores, respectively.

2. THEORETICAL TREATMENTS

Phase separation occurred via spinodal decomposition within the spinodal region in the $Na_2O-B_2O_3-SiO_2$ system.[21] The microstructural change is considered to take place via two stages. First, a metastable glass in the spinodal region undergoes phase separation into a SiO_2-rich phase and a borate-rich phase via a thermodynamic process. Second, the phase separated structure grows in order to decrease the total interface area between the two phases, a kinetic process. Figure 1 shows the two-step procedure proposed in this study from the point of view of thermodynamics.[22] The glass is allowed to phase separate at T_1 and then elevate to T_2 for another equilibrium. In this section, the two stages at T_1 are dealt with first, and then the results will be extended for the second step at T_2. During the phase separation, the highly viscous SiO_2-rich phase evolves into a solid phase,[23] suggestive of a dynamically asymmetric system.[24] We limit ourselves to structural growth based on a dissolution-growth process in the borate-rich phase.

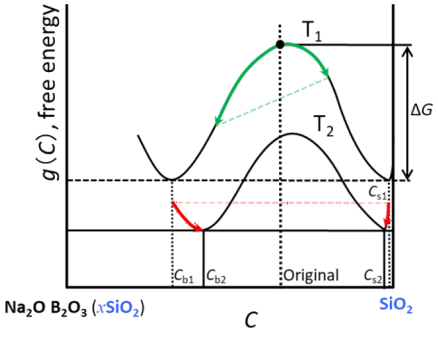

Figure 1. Schematic illustration of two thermodynamic processes at T_1 and T_2 in the two-step procedure, where $T_2 > T_1$. Two curves indicate the compositional dependences of free energy at T_1 and T_2, respectively.[22] C_{b1} and C_{b2} are the concentrations in the borate-rich phase, and C_{s1} and C_{s2} are those in the SiO_2-rich phase at T_1 and T_2 at the immiscibility gap, respectively. At T_2, there is an overall shift in the peak region because of the asymmetric nature of the immiscibility dome (see Figure 8). Green arrows indicate the first thermodynamic process of phase separation via compositional fluctuation, and ΔG is the negative change in free energy by the phase separation. Red arrows show the second thermodynamic process when elevated to T_2 from the equilibrium at T_1.

2.1. Phase Separation by Spinodal Decomposition

As for the phase separation by spinodal decomposition, according to a general derivation given by Cahn and Hilliard,[25] the minimum wavelength of compositional fluctuation, λ_c, is expressed using eq 1.[6,26]

$$\lambda_c = \left[-\frac{8\pi^2\kappa}{\frac{\partial^2 g(C)}{\partial C^2}} \right]^{1/2} \tag{1}$$

where κ is a positive coefficient related to the gradient energy $[\kappa(\nabla C)^2]$, $g(C)$ is the function of free energy, and C is the concentration of composition. The thermodynamic process at T_1 in Figure 1 accounts for normal spinodal decomposition. When $\partial^2 g(C)/\partial C^2 < 0$ at $C_{original}$ (the concentration of glass), a compositional fluctuation with a wavelength of $>\lambda_c$ leads to the spinodal decomposition. A high-silica phase was formed with the progress of phase separation, in which the content of B_2O_3 and Na_2O was lowered toward ~5 wt % (C_{s1} ~95 wt %),[27] leading to the sharp interface. In this study, the theory was extended to depict the average periodic distance with thermodynamic parameters and kinetic variables relevant to heat treatments for phase separation. Following the treatment of the gradient energy,[7,26] if the phase separation proceeds to a high degree with little loss in diffusion, the interfacial energy should arise at the expense of the reduction of free energy. Based on a scaling law for spinodal structure, the period of phase separation is related to ΔG as follows:

$$d = -\frac{\alpha\gamma V_m}{\Delta G} \tag{2}$$

where d is the periodic distance, α is a coefficient relevant to the ratio of interface area to volume [area/volume = $\alpha(1/d)$], and γ and V_m are the interfacial energy and the molar volume of the SiO_2-rich phase, respectively. ΔG is the negative change of free energy per mole by the phase separation (Figure 1). Since $-\Delta G$ increases with the undercooling from the upper consolute temperature (T_c), d decreases with a decrease of the temperature.

The degree of phase separation could be assessed from the stability of the SiO_2-rich phase when subject to etching or leaching.[28] To our knowledge, provided the SiO_2-rich phase was developed to high degrees in typical glass compositions,[29,30] porous bulks of silica were available irrespective of the high capillary force due to the nano pores. According to Takamori and Tomozawa,[23,31] long heat-treatment times were required to attain the equilibrium composition with decreasing temperature on the basis of increased viscosities due to the interconnected SiO_2-rich phase. Once $-\Delta G$ is consumed in this way, the spinodal structure undergoes growth in the second stage.

2.2. Growth of the Spinodal Structure

It has been reported that the periodic distance and radius of pores varied with time (t) following a relation of $\propto t^{1/3}$ during the growth under a diffusion-controlled process.[32−35] This relation has been proven in the correlation length in optical scattering,[36] small-angle X-ray scattering,[37] and AFM analysis on the fractured surface.[38−40] This kinetics of growth resembles the growth of particles in metals[41] and Ostwald ripening under dilute conditions.[42,43] It is accepted that the reduction of the

https://doi.org/10.1021/acsphyschemau.4c00060
ACS Phys. Chem Au 2024, 4, 696−706

total interfacial energy works as the driving force for the growth. Haller anticipated a relation of $S \propto t^{-1/3}$ (S: interfacial area) in the rearrangement of the two phases by a particle model.[44] However, a convincing mechanism of diffusion is still needed for the interface between two interconnected phases.

It was found that some of the interface of the interconnected pores resembles cylinder in shape and the pores were present in the sharp distributions of diameter in etched samples.[14] As to the influence of curvature of interface, the concentration of SiO_2 in the borate-rich phase can be expressed using the Thomson–Freundlich (Kelvin) equation.[45,46]

$$S_{\mathrm{eff}} = S_0 \exp\left(\frac{2\gamma V_{\mathrm{m}}}{RTr_{\mathrm{eff}}}\right) \tag{3}$$

where S_{eff} and S_0 are the solubilities of the SiO_2-rich phase corresponding to the interface with the effective curvature radius and the flat interface, respectively. r_{eff} is the effective curvature radius of the interface from the side of the SiO_2-rich phase. That is, the chemical potential (μ_{eff}) varies with r_{eff} according to eq 4.[45,46]

$$\mu_{\mathrm{eff}} = \mu_0 + \frac{2\gamma V_{\mathrm{m}}}{r_{\mathrm{eff}}} \tag{4}$$

In fact, the practical pores are interconnected in a complicated manner, and therefore there is a distribution in r_{eff} in the borate-rich phase. This probably arises from a high fraction of the two phases in volume and from a difference in mobility between the two phases during the phase separation. The distribution persists even during growth, giving rise to a gradient of the chemical potential in the borate-rich phase, which should derive the movement of SiO_2 among silica skeletons.

Figure 2 shows the schematic mechanism proposed to interpret the growth of the spinodal structure. $q(r)$ is defined as the growth of SiO_2 in moles per area at the interface. For convenience of understanding, a large amount of the borate-rich phase is assumed to be in equilibrium with the SiO_2-rich phase with a curvature of $\bar{r}$. The movement of SiO_2 $[q(x)]$ toward the interface is expressed by introducing a term of r^2/x^2 as an effect of the inverse-square law. This is necessary for a spherical nature of interface at the growth front and also for a condition of flux in the steady diffusion. To derive $q(r)$ at the interface, eqs 5-I and 6-I are arranged from the basic diffusion equation of $q(x) = -cB(\mathrm{d}\mu/\mathrm{d}x)$, so that both sides yield positive changes.

When $r < \bar{r}$,

$$\int_r^{\bar{r}} -q(r)\frac{r^2}{x^2}\mathrm{d}x = \int_r^{\bar{r}} -cB\mathrm{d}\mu \tag{5-I}$$

$$q(r)r^2\left(\frac{1}{\bar{r}} - \frac{1}{r}\right) = -cB \times 2\gamma V_{\mathrm{m}}\left(\frac{1}{\bar{r}} - \frac{1}{r}\right) \tag{5-II}$$

$$q(r) = -\frac{1}{r^2}cB \times 2\gamma V_{\mathrm{m}} \tag{5-III}$$

When $r > \bar{r}$,

$$\int_{\bar{r}}^{r} q(r)\frac{r^2}{x^2}\mathrm{d}x = \int_{\bar{r}}^{r} -cB\mathrm{d}\mu \tag{6-I}$$

$$-q(r)r^2\left(\frac{1}{r} - \frac{1}{\bar{r}}\right) = -cB \times 2\gamma V_{\mathrm{m}}\left(\frac{1}{r} - \frac{1}{\bar{r}}\right) \tag{6-II}$$

$$q(r) = \frac{1}{r^2}cB \times 2\gamma V_{\mathrm{m}} \tag{6-III}$$

where c and B are the concentration and mobility of SiO_2 in the borate-rich phase contributing to the diffusion, respectively. In eqs 5-III and 6-III, $q(r)$ varies simply as a function of $1/r^2$.

On the above assumption, the curvature of the interface continues to change with the growth. The concentration of SiO_2 in the borate-rich phase is being kept in the steady state via the two processes (precipitation and dissolution), and little growth occurs at $\bar{r}$. Hence, the interface having $\bar{r}$ appears to play a role as a constraint for the variation of the curvature. By assuming a curved interface with circular symmetry, the geometric description of point S is shown in Figure 3, through which there is a region of the interface having the curvature radius of $\bar{r}$ around the axis of symmetry with a height of H in the perpendicular direction.

Equation 7 is derived by using the relations of $H^2 = \tau \times (2r - \tau)$ and $\mathrm{d}H^2 = 0$.

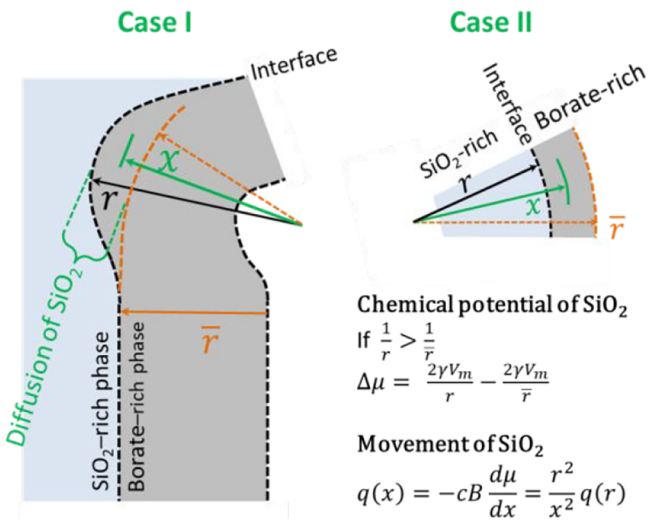

Figure 2. Illustration of the diffusion of SiO_2 from silica skeletons during the growth of the spinodal structure. r: negative in case I; r: positive in case II. The chemical potential of SiO_2 is expressed by relating to the radius of curvature of r at the interface for the silica skeletons and that of $\bar{r}$ for the borate-rich phase in a steady state, respectively. The movement of SiO_2 $[q(x)$ at $x]$ obeys the inverse-square law.

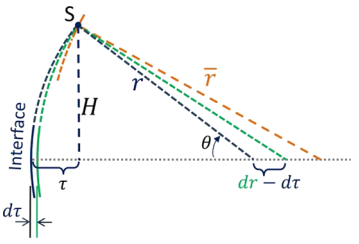

Figure 3. Description of the change of r during the growth of the spinodal structure. A geometrical point S indicates the position of a region of interface where the height is H and the interface has the curvature of $\bar{r}$. The interface moves with $\mathrm{d}\tau$ accompanied by a change of $\mathrm{d}r$, obeying a basic relation of $H^2 = \tau \times (2r - \tau)$. θ is a parameter of angle characteristic of an area that undergoes either growth or dissolution.

https://doi.org/10.1021/acsphyschemau.4c00060
ACS Phys. Chem Au 2024, 4, 696–706

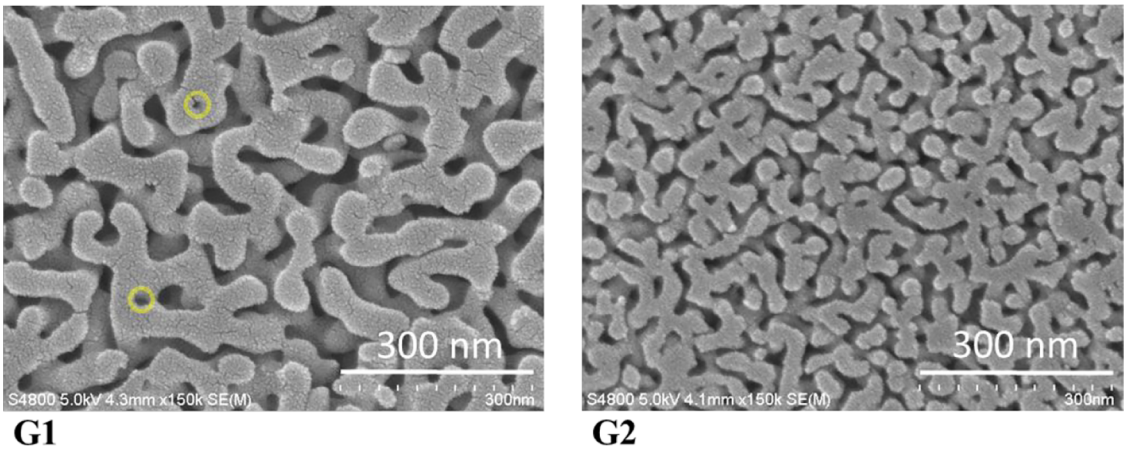

Figure 4. Micrographs of G1 and G2 glasses heat-treated at 560 °C for 50 h. Yellow circles indicate small pores that resulted from the borate-rich phase existing in the SiO_2-rich phase.

$$d\tau = \frac{2}{\left[-\frac{H^2}{\tau^2}+1\right]}dr = \frac{2}{\left[-\frac{1}{\left(\tan\frac{\theta}{2}\right)^2}+1\right]}dr \tag{7}$$

where τ is the depth of the interface from the plane of the region having the curvature of $\overline{r}$. θ is the angle characteristic of the area for growth or dissolution. From the geometric point of view, for a cylinder terminated by semispheres, $\theta \sim \pi/2$, and in the case of a cross of two cylinders with an angle of $\pi/2$, $\theta \sim \pi/4$. Here, θ is considered an important parameter for the description of growth or dissolution under the condition of the distribution of curvature, since $\overline{r}$ varies practically with the growth.

The growth of the SiO_2-rich phase at the interface $(-d\tau)$ can be related to $q(r)$ (mole per area and per period of time) by eq 8, and eq 9 is attained for the change of r from eq 7. As a result, eqs 10-I and 10-II are obtained by incorporating eqs 5-III and 6-IIIinto eq 9, arranging a term of $3r^2dr$ for the left side and integrating them with a change from r_0 to r.

$$-\frac{d\tau}{V_m} = q(r)dt \tag{8}$$

$$dr = -\frac{1}{2}\left[-\frac{1}{\left(\tan\frac{\theta}{2}\right)^2}+1\right]V_m q(r)dt \tag{9}$$

$$r^3 - r_0^3 = \left[-\frac{1}{\left(\tan\frac{\theta}{2}\right)^2}+1\right]3cB\gamma V_m^2 t,\ r < \overline{r} \tag{10-I}$$

$$r^3 - r_0^3 = -\left[-\frac{1}{\left(\tan\frac{\theta}{2}\right)^2}+1\right]3cB\gamma V_m^2 t,\ r > \overline{r} \tag{10-II}$$

where t is the time for the growth. Equation 10-I should be responsible for the growth of the borate-rich phase, which determines the pores in etched samples. The diameter of a cylinder of the borate-rich phase ϕ may be approximated to $2H$ as follows:

$$\phi \sim 2H = 2|r|\sin\theta \tag{11}$$

By combination of eq 10-I with eq 11, the growth of the borate-rich phase can be expressed as eq 12.

$$\phi - \phi_0 = 24\left|\frac{1}{\left(\tan\frac{\theta}{2}\right)^2}-1\right|(\sin\theta)^3 cB\gamma V_m^2 t \tag{12}$$

In this study, the spinodal porous structure is described by means of average periodic distance d and porosity ν (see Section 3). d can be related to ϕ by a relation of $d = \sqrt{\pi/(4\nu)}\,\phi$, and therefore d increases with time during the growth as follows:

$$d^3 - d_0^3 = At,$$
$$A = 3\pi^{3/2}\left|\frac{1}{\left(\tan\frac{\theta}{2}\right)^2}-1\right|(\sin\theta)^3\frac{1}{\nu^{3/2}}cB\gamma V_m^2 \tag{13}$$

where A is the kinetic parameter for the growth based on the borate-rich phase. On the other hand, if attention is paid to a cylinder form of the SiO_2-rich phase, the rearrangement would be possible by assuming the growth of SiO_2 onto the surface of cylinders by eq 10-II. Equation 14 could be available from the average width of skeletons (ϕ') by using a relation of $d = \sqrt{\pi/[4(1-\nu)]}\,\phi'$.

$$d^3 - d_0^3 = A't,$$
$$A' = 3\pi^{3/2}\left|\frac{1}{\left(\tan\frac{\theta}{2}\right)^2}-1\right|(\sin\theta)^3\frac{1}{(1-\nu)^{3/2}}cB\gamma V_m^2 \tag{14}$$

If the second mechanism by eq 10-II were true, the concentration of SiO_2 in the borate-rich phase would be supersaturated from the shape of the cylinders ($\overline{r}$: positive). The growth of SiO_2 should take place preferentially onto the concave interface. In fact, the concave areas are observable yet in all the spinodal silica. Therefore, eq 13 seems more suitable to treat the growth of the present spinodal structure that is driven by a decrease in the total interfacial energy. In the situation of $r < 0$, θ is smaller than $\pi/2$ in eq 10-I and larger than $\pi/2$ in eq 10-II. This means that the dissolution occurs from a smaller region via eq 10-I, whereas dissolved silica is being deposited onto a larger

https://doi.org/10.1021/acsphyschemau.4c00060
ACS Phys. Chem Au 2024, 4, 696−706

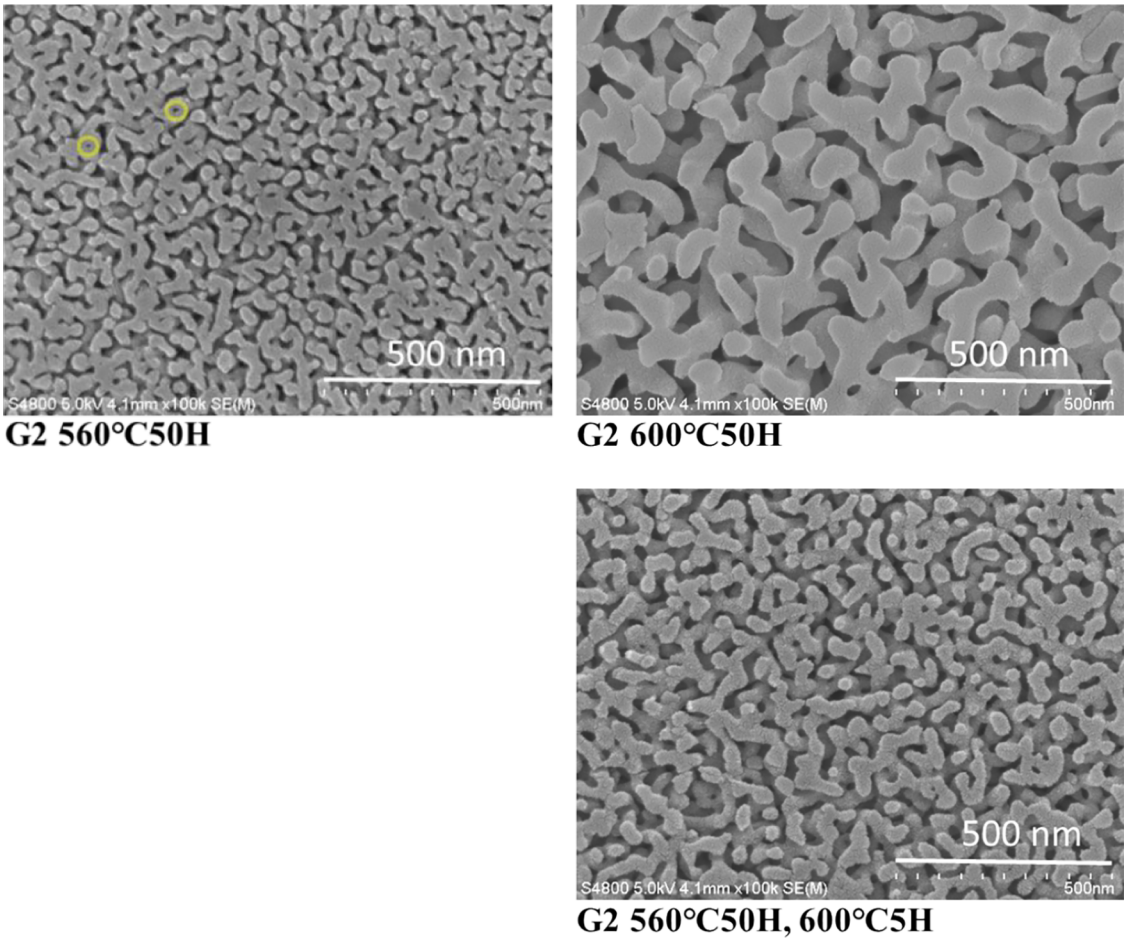

Figure 5. Micrographs of G2 glasses relevant to the two-step process. The upper ones were heat-treated at 560 and 600 °C for 50 h, respectively, and the bottom one was heat-treated at 560 °C for 50 h and at 600 °C for 5 h. Yellow circles indicate little pores that resulted from the borate-rich phase existing in the SiO_2-rich phase.

area via eq 10-II. At the growth front of the borate-rich phase, some silica skeletons become relatively narrow and further broken, leading to convex surfaces. This process creates new interfaces where $1/r > 1/\bar{r}$ $(r < \bar{r})$. With an increase of $1/r$ or $|r|$ in the region of curvature by eq 10-II where $1/\bar{r} > 1/r$ $(r > \bar{r})$, $1/\bar{r}$ or $|\bar{r}|$ increases, maintaining a distribution of the curvature. If there is an ideal cylinder with a length, the borate-rich phase inside tends to be kept in equilibrium with the local interface $(1/r)$. The curvature $(1/r)$ is eventually left under $1/\bar{r}$, which probably allows SiO_2 to deposit onto the interface inside the cylinder. Namely, there is a rearrangement of SiO_2 in the vicinity of the surface, which deviates from the condition for the inverse-square law. Therefore, the uneven surfaces including little cylinders of borate-rich phase inside (see little pores notated by yellow circles in Figures 4 and 5) may be regarded as the transitional textures of the interface, and r in eqs 10-I and 10-II is considered to be the parameter of a macroscopic range, which is characteristic of the growth of borate-rich phase as suggested in Figure 3.

Since $|\bar{r}| = \phi$ for the surface of a cylinder, ϕ becomes $2\phi \sin\theta$ with the growth of the borate-rich phase. In fact, we have investigated Kelvin's diameters (φ) of spinodal silica by adsorbing/desorbing experiments with changing humidity, and $\varphi_{ad}/\varphi_{de}$ was found to be ~1.7,[14] strongly suggestive of a serial distribution of two diameters. Such a result seems in agreement with the factor of 2 sin θ, if assuming $\theta \sim \pi/3$.

The diffusion was also attempted by assuming a uniform diffusional length other than the inverse-square law, and the relations of $\propto t^{1/2}$ were obtained. However, the viscosity of the borate-rich phase is still high in the temperature range of phase separation. Such a mechanism based on the diffusion of SiO_2 across a thin diffusion layer near the interface seems in disagreement with the growth of spinodal structure, especially under the confined condition.

If there is an ideal transition from the first stage to the second stage, d in eq 2 should be d_0 in eq 13, and t in eq 13 is the time for growth from d_0 to d. For convenience, d_0 is defined as the minimum periodic distance after the first stage of spinodal separation. When the temperature is elevated to T_2 in the two-step process in Figure 1, the glass undergoes the second thermodynamic process. Due to the asymmetric nature of the immiscibility gap,[3] the SiO_2 concentration of the borate-rich phase varies from C_{b1} to C_{b2}, and the fraction of borate-rich phase increases probably with little change in d (also see Figure 8).[47] After equilibrium, the structure grows again, and the average periodic distance is expressed as follows.

$$t' = t - t_1 + d_1^3/A \tag{15}$$

$$d^3 = At' \tag{16}$$

where A is a parameter inherited from eq 13. t' is the modified time. t and t_1 are the time practically elapsed in the second step

https://doi.org/10.1021/acsphyschemau.4c00060
ACS Phys. Chem Au 2024, 4, 696−706

Table 1. Glass Compositions, Tg, and Conditions of Heat Treatments

						conditions				
							heat treatments for phase separation			
	compositions (wt %)						one-step (first step)		second step	
glasses	SiO_2	B_2O_3	Na_2O	Al_2O_3	Tg/°C	annealing	T_1/°C	t/h	T_2/°C	t/h
G1[a]	59.9	31.0	9.1	0	508	513 °C	560	50		
G2[a]	59.0	30.5	9.0	1.5	490	495 °C	520	50[d]		
								50	600[b]	5
							540	50[d]		
								50	600[b]	5
										10
										15
							560	50[d]		
								50	600[b]	5
							600[b]	25[e]		
								50[d,e]		
								100[e]		
G3[c]	62.5	27.3	7.2	3.0	478	485 °C	500	24		
							525	24		
							560	24		
G4[c]	62.9	27.9	9.2	0	508	515 °C	600	50		
							620	50		
								100		
								150		

[a]The ratios of Na_2O and B_2O_3 to SiO_2 are unchanged in G1 and G2 glasses. [b]600 °C is the equilibrium temperature for the growth of spinodal structure in G2 glass. [c]G3 and G4 glasses are included for the normal tendency of spinodal structure by a one-step process. [d]Series I (G2 glass, one-step process): the temperature varies from 520 to 600 °C with the period of 50 h. [e]Series II (G2 glass, one-step process): the period of time varies from 25 to 100 h at 600 °C.

and the time taken to attain equilibrium, respectively. d_1 is the average periodic distance immediately after reaching the equilibrium.

The two equations can be regarded as general formulas for the normal spinodal separation by a one-step process. In such a case, t_1 is the time for the glass to yield the phase-separated state, as described in Section 2.1, and d_1 is d_0 as just mentioned above. Equations 2, 15, and 16 provide the basis for the analysis of spinodal decomposition by a two-step process.

3. EXPERIMENTAL SECTION

Table 1 shows the batch compositions of glasses employed in this study and the experimental conditions of annealing and heat treatments for the phase separation. The glass compositions were decided by referring to literatures,[29,32,48] and the ratios of B_2O_3 and Na_2O to SiO_2 were unchanged in G1 and G2 glasses with an aim of verifying the role of Al_2O_3 in the interfacial energy (γ). High silica (F2 grade, Nitchitsu Co.), $B(OH)_3$ (Optibor TG, U.S. Borax), and Na_2CO_3 (particle form, Tokuyama Co.) were used for the sources of SiO_2, B_2O_3, and Na_2O, and the purities were higher than 99.6, 99.9, and 99.2%, respectively. Batches with weights of 10 or 20 kg were melted by using Pt crucible with a cover of Pt plate at 1450 °C for 3−4 h and poured out to a mold. The glass blocks were put into an electric furnace preheated at the annealing temperatures, and then the temperatures of the furnace were allowed to cool down immediately at a rate of 1 °C/min.

The glass samples thus obtained were cut into plates with a size of 30 × 30 × 1 mm, and both sides of the plates were polished to an optical grade. Prior to the heat treatments for phase separation, the glass transition temperatures were investigated by thermomechanical analysis (TMA) by using silica glass as the reference, and the uncertainty in Tg was estimated to be within ±5 °C. As to the states of glasses prior to the heat treatments for phase separation, the glass surfaces were observed after etching at 90 °C in 1 N HNO_3, and no surface texture of phase separation was observed.

As for the development of durability, a comparison was made between the G1 and G2 glasses (not shown in Table 1). The two glasses were heat-treated at 500 to 560 °C for 10 to 24 h, respectively, and the stability of the SiO_2-rich phase was investigated by exposure to etching.

In Table 1, temperatures higher than the transition temperatures were chosen for phase separation with the primary aim of durability for all the samples. For the systematic analysis of two stages, both one-step and two-step processes were applied for the G2 glass, in which a final equilibrium was set at 600 °C. In the one-step process, the glass was heat-treated at 520 to 600 °C for 50 h (series I; see the footnote in Table 1) and heat-treated for 25, 50, and 100 h at 600 °C (series II) with intents to clarify the effect of ΔG in the initial stage (eq 2) and the time dependence in the latter growth (eq 13), respectively. In the case of the two-step process, the samples were heat-treated at 520, 540, or 560 °C for 50 h, and then at 600 °C for 5 h. From the first step at 540 °C for 50 h, two additional samples were prepared by prolonged heat treatments at 600 °C for 10 and 15 h in the second step. In the G3 and G4 glasses, the samples were prepared by a one-step process for a normal tendency in porous glasses, in which heat-treatment temperature is the main parameter with an attention on the concentration of Al_2O_3.

Prior to the etching, the heat-treated samples were polished for 5 min by a grinding machine (MA-300, Musashino Denki) using CeO_2 powder at a load of about 5 N over an area of 30 × 30 mm. During the polishing, a skin SiO_2 layer on the surfaces that was generated due to the volatilization of Na_2O and B_2O_3 during high-temperature processes[30,51] was removed. During the etching, these samples were exposed to 500 mL of 1 N HNO_3 for 24 h at 90 °C. Finally, they were rinsed several times with pure water and dried at 40 °C for 2 to 5 h.

All of the porous surfaces were observed by a scanning electron microscope (FESEM S-4800, Hitachi). Two methods were used to analyze the micrographs (Supporting Information). First, lines were drawn among the middle points of silica skeletons over large areas of the images, and the number of periods between adjacent uppermost surfaces along the lines was counted. The average periodic distances (d) were obtained by dividing the total lengths of lines (L) with the numbers of periods (N). The stereological analysis was based on the

https://doi.org/10.1021/acsphyschemau.4c00060
ACS Phys. Chem Au 2024, 4, 696−706

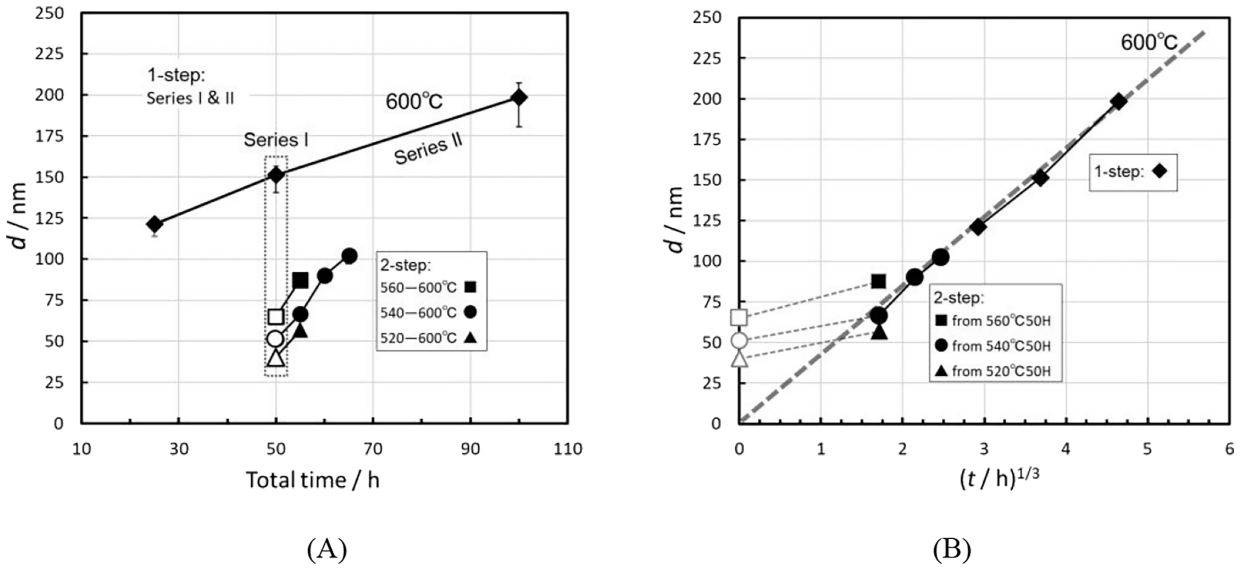

Figure 6. Average periodic distances between skeletons for the G2 glasses. (A) Average periodic distances are plotted as a function of the total time of the heat treatments. (B) Average periodic distances are plotted as a function of $t^{1/3}$, and t is the heat-treatment time at 600 °C. The data in the first steps at 520, 540, and 560 °C for 50 h are indicated by open marks as the references for the samples by the two-step process.

facts that silica skeletons were distributed randomly in the spinodal structure and that the average distances should converge true values with increasing N. Second, the images of micrographs were analyzed by the software of ImageJ.[52] They were transformed to binary ones by setting the threshold brightness in Auto mode. The fractions of dark areas (f) were obtained as the measure of porosity. The average widths of skeletons (w) were also estimated by taking the average of the minor widths of the ellipses that were transformed from the white areas.

4. RESULTS

As for the kinetics of phase separation, the glass transition temperatures were investigated for the four glasses, and the results prior to phase separation are listed in Table 1.[49] Tg clearly decreased with the addition of Al_2O_3, which seems to be a characteristic of sodium borosilicate glasses having molar ratios of $[Al_2O_3]/[Na_2O]$ lower than 1[50] with a form of $Na - AlO_4$ (see Discussion).

Figure 4 shows the micrographs of G1 and G2 glasses that were prepared at 560 °C for 50 h. The pores resulted from the borate-rich phase being etched. By stereological analysis, the average periodic distances between skeletons were 101 to 65 nm for G1 and G2 glasses, respectively. In addition to the pores characteristic of the interconnected borate-rich phase, there were small pores notated by yellow circles, which resulted from the borate-rich phase existing in the SiO_2-rich phase. When G1 glass was heat-treated at 500 to 560 °C within 24 h and then exposed to the etching, it appeared weak and tended to yield a layered residue of the SiO_2-rich phase, resembling the phenomena in literature.[29,48] This means that the durability of G1 glass at 560 °C was attained between 24 and 50 h. On the other hand, the G2 glass yielded durable porous structures when it was phase separated for more than 24 h above 540 °C. At 520 °C, bright images with a spinodal structure were obtained in the SEM observation, and no difficulty was caused in the subsequent analysis. Hence, the G2 glass in Figure 4 should have undergone growth in spite of the small feature.

The typical micrographs relevant to the two-step process in the G2 glass are shown in Figure 5. The average periodic distance between skeletons varied depending on the respective heat treatments. The width of skeletons of the G2 glass heat-treated by the two-step process was narrow compared with the glass by the one-step process at 600 °C for 50 h, and the porosity, however, was elevated to the same level due to the second heat-treatment at 600 °C for 5 h.

In Figure 6A, the average periodic distances (d) obtained by stereological analysis are plotted as a function of the total time of heat treatments for G2 glasses. In series I, d changed from 151.3 to 40.1 nm with a decrease of temperature from 600 to 520 °C. In series II, it increased from 121.2 to 198.5 nm with the time at 600 °C. As to the errors in d, there may be an overestimation, which arose from lost uppermost surfaces (islands) during the etching (Supporting Information). If one assumes that one uppermost surface along the lines has been lost during the etching, the overestimation is estimated to be $1/N$. On the other hand, when considering L with a change from $N - 1$ to N, the deviation resulted directly from the individual distance. In fact, the individual distances had a range of 1/2 to 2-fold the average periodic distance for each sample. Therefore, the deviation in d due to L was estimated to be $-1/(2N)$ to $1/N$. If the main factors were considered for both sides, the error in d ranged from $-1/N$ to $1/(2N)$. In this analysis, the magnification was 150 k in the micrographs, and N ranged from 11 to 48 depending on the average periodic distance. The errors in d were less than 10%.

In Figure 6B, the average periodic distances are plotted as a function of $t^{1/3}$, and t is the heat-treatment time at 600 °C. Clearly, the glasses that underwent growth at 600 °C fell into the relation of $d \propto t^{1/3}$, and there were some scatterings in the samples by the two-step process at 5 h ($t^{1/3} = \sim 1.7\ h^{1/3}$).

The results of f and w obtained by ImageJ analysis are shown in Figure 7. The blue symbols indicate the results of G2 glass by the two-step process, where the heat-treatment temperatures were 520 to 560 °C in the first step and 600 °C in the second step, respectively. Porous samples derived from G3 and G4 glasses are also included for the normal tendency in structure by the one-step process. For comparison, the typical results by ImageJ in G2 glass are listed in Table 2 with the corresponding data of d obtained by the stereological analysis. It was found that the fractions of dark area (f) were about 20% lower than the practical porosities (ν) calculated from the reflection in the

https://doi.org/10.1021/acsphyschemau.4c00060
ACS Phys. Chem Au 2024, 4, 696−706

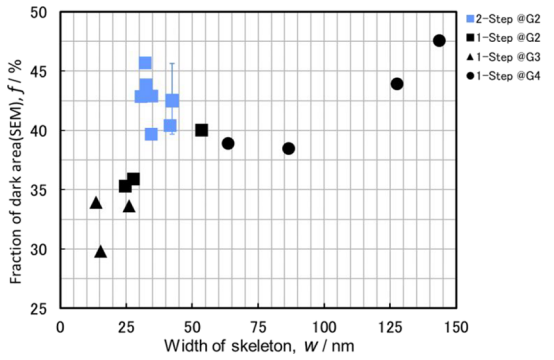

Figure 7. f vs w from ImageJ analysis. Blue symbols indicate the results of G2 glasses by the two-step process. G3 and G4 glasses are included for the normal tendency by one-step process.

visible region.[53] In the ImageJ analysis, some skeletons beneath the polished surface were transformed into white regions and included as the top surface (see the Supporting Information). This was attributed to the fact that the SEM images had not enough contrast for distinguishing the upmost surface completely from the silica skeletons beneath the surface. By using a relation of $w = d \times (1 - \nu)$ (ν: porosity) and using ν of 62% at 600 °C obtained by the optical reflectivity, the widths of skeletons by ImageJ analysis were judged to be overestimated by a factor of ∼1.2 for the glasses by the two-step process for a range of d from 60 to 100 nm. Furthermore, the scatterings in f were analyzed on the G2 glasses with equilibrium at 600 °C because their porosities should be on the same level. These glasses showed the average f of 42.2% with the scattering from 39.6 to 45.6%, which was indicated in Figure 7 as the representative error in f. The scattering in w resulted from the conditions of SEM observation as in f, but no data were available for the similar analysis, which is outside the scope of the present study.

As for the normal tendency by a one-step process (Figure 7 and Table 2), the porosity increased with the heat-treatment temperature, accompanied by the enlargement of structure (see the conditions in Table 1), which remains to be included in future with various porous silicas by one-step process having polished surfaces. A similar change with temperature was reported by Haller et al.[5] on a glass close to G1, and the volume of borate-rich phase changed from 30 to 65% at 550 to 715 °C. However, the porosities were lower compared with the present study under the similar conditions. Such a difference in porosity may result from an overestimation of the SiO_2-rich phase in the transcription to polyester sheet in the literature, resembling the present ImageJ analysis.

5. DISCUSSION

In the present system, the stable SiO_2-rich phase with a well-developed interface is attained by concentrating SiO_2 from neighboring regions (the borate-rich phase), which occurs from the infinitesimal compositional fluctuation over a range of $\geq\lambda_c$, and continues lowering the borate component (Na_2O B_2O_3) toward an equilibrium value. This results in solidification due to the increase of viscosity in the interconnected SiO_2-rich phase. On the other hand, the surrounding borate-rich phase remains fluid due to incoming borate components from the SiO_2-rich phase, enabling an appreciable mobility of SiO_2 in it. Then, the movement of SiO_2 in the borate-rich phase becomes dominant in the structural growth. The dissolution−precipitation process (eq 13) is assumed to account for the growth of the spinodal structure at the second stage.

In the first stage of phase separation, λ_c and d are determined by the glass composition and undercooling ($-\Delta G$) via eqs 1 and 2 at a given temperature. As suggested by Charles,[21] the spinodal separation begins easily (e.g., below 1 min), because there is no thermodynamic barrier for it as seen in Figure 1. Then, the phase separation in composition proceeds toward the equilibrium, so that the concentration of the borate component in the SiO_2-rich phase decreases to ∼5 wt % to yield the stability against etching. Therefore, there is a desirable heat-treatment time to attain good stability. In the present study, however, the conditions of phase separation were investigated by focusing on the desirable temperatures for the stability with the heat-treatment time of 24 h, and they were found to be higher than 560 °C for the G1 glass, ∼520 °C for the G2 glass, and ∼500 °C for the G3 glass.

As seen in Figure 4, due to the addition of Al_2O_3, the periodic distance decreased by 35% compared to that of the G1 sample under the same heat-treatment condition. From the point of view of kinetics, the phase separation should occur easily with the addition of Al_2O_3 by judging from the decrease in Tg, and therefore t_1 in eq 15 should be shortened in the one-step process and the kinetic factor of B in eq 13 may increase to some degree in the G2 glass. If there were no changes in κ and γ in eqs 1 and 2 between the two glasses, the average periodic distance should have grown to a larger value in G2 glass. Hence, the Al_2O_3-induced decrease in d is explainable only by assuming a decrease in κ and γ. According to a compositional study,[27] the contents of Al_2O_3 decreased to less than 1/10 in porous silica after etching. Hence, Al_2O_3 tended to be either enriched in the borate-rich phase or present at the interface during phase separation and growth. Minamiyama et al. investigated the proton conductivity in porous silica derived from Al_2O_3-doped $Na_2O-B_2O_3-SiO_2$ glasses at 585 °C.[54] The proton conductivity increased with the introduction of Al_2O_3 in original glasses toward 2 mol %, and Al^{3+} was inferred to exist on the surface of spinodal pores as

Table 2. Typical Analysis Data of Porous Samples in the G2 Glass[a]

	one-step process				two-step process (after the first step at 540 °C for 50 h)		
	temperatures (for 50 h)				time (in the second step at 600 °C)		
parameters	520 °C[d]	540 °C	560 °C	600 °C	5 h	10 h	15 h
d (nm)[b]	40.1	51.2	65.1	151.3	66.6	90.1	102.4
w (nm)		24.7	27.7	53.7	32.6	41.8	42.4
f (%)[c]		35.2	35.8	40.0[c]	43.7[c]	40.4[c]	42.4[c]

[a] d: average periodic distances determined by the stereological analysis. w: the width of silica skeletons; f: the fractions of dark areas, by ImageJ analysis. [b] The error in d was less than 10%. [c] The factions of dark areas (f) of the glasses with the equilibrium at 600 °C ranged from 39.6 to 45.6% with the average of 42.2%. [d] Only bright image was obtained for the sample heat treated at 520 °C, which had no contrast enough for ImageJ analysis.

https://doi.org/10.1021/acsphyschemau.4c00060
ACS Phys. Chem Au 2024, 4, 696−706

Brønsted acid in a form of H−AlO_4. A structural study of ^{27}Al NMR indicated that Al^{3+} existed in the tetrahedra of AlO_4 in place of BO_4 and increased the compatibility of the silica network with the −B−O− network.[55] Therefore, a fraction of Al_2O_3 existed at the interface during the phase separation and the growth in G2 glass and played a role of reducing κ and γ in eqs 1 and 2. As a result, d decreased with the addition of Al_2O_3 in phase separation. According to the mechanism for the stability of the SiO_2-rich phase, the reduction of d in eq 2 should facilitate the establishment of durable silica skeletons at the first stage, although there is little knowledge of the role of Al_2O_3 in the removal of the borate component from the SiO_2-rich phase.

The range of the heat-treatment temperature for the phase separation in the G2 glass became wider with the benefit from the decrease of Tg. This situation was also true in the G3 glass. In other words, the increased mobility and reduced interfacial energy caused by the addition of Al_2O_3 facilitated the phase separation at lower temperatures, leading to the reduction of λ_c and d. These effects can be recognized in the results of series I in the G2 glass in Figure 6A and in the region of the spinodal structure of G3 glass in Figure 7. Al_2O_3 is an intermediate oxide in normal glass systems and fortifies the glass as a network former. In fact, the addition of Al_2O_3 was considered to suppress the immiscibility and increase the chemical vulnerability of glasses.[55,56] The suppression of phase separation was based on the fact that the scattering of light decreased with the addition of Al_2O_3 in the resultant glasses.[5,55] In this study, however, Al_2O_3 plays a role in enhancing the phase separation conversely in the establishment of durable silica skeletons. If the Al_2O_3-induced decrease in γ is taken into consideration with eq 2, both phenomena should result from the reduction of d. In addition to Al_2O_3, metal oxides such as Fe_2O_3, TiO_2, CeO_2, and SnO_2 were also investigated with molar ratios corresponding to 1.5−2 wt % of Al_2O_3. However, they showed no remarkable reduction in the periodic distance under similar conditions, as reported recently for TiO_2.[57]

During the etching, the borate-rich phase was taken out completely even with SiO_2 dissolved in it, and therefore, the fraction of borate-rich phase in volume led to the resultant porosity. As described in the following, the fraction of borate-rich phase depends on the glass composition and the equilibrium temperature.[58] The porosity could be controlled effectively by changing the equilibrium temperature, as seen in Figure 5 and Table2 for G2 glass. On the other hand, the average periodic distance (d) depended on both the thermodynamic and kinetic processes so far.

Figure 8 shows the schematic diagram of the two-step process focused on the fraction of borate-rich phase, where the Al_2O_3 component is omitted for convenience. When elevated to T_2, the SiO_2 concentration in the borate-rich phase turns into an unsaturated state, and SiO_2 starts to diffuse into it from the surrounding SiO_2-rich phase. This can be recognized in the change of porosity in the micrographs in Figure 5 and in the change of the fraction of dark area in Figure 7, in correspondence with the changes of temperature from 540 and 560 to 600 °C. Meantime, once the SiO_2 concentration reaches the immiscibility dome in correspondence to C_{b2} in Figure 1, the skeletons undergo growth again. It should be mentioned that the borate component (Na_2O B_2O_3) in the SiO_2-rich phase may be difficult to reach equilibrium due to the solid nature. Nevertheless, the equilibrium concentration of the borate component remained essentially at ∼5 wt %[27] in the temperature range of phase separation; the influence on the fraction of borate-rich phase at T_2 may be negligible.

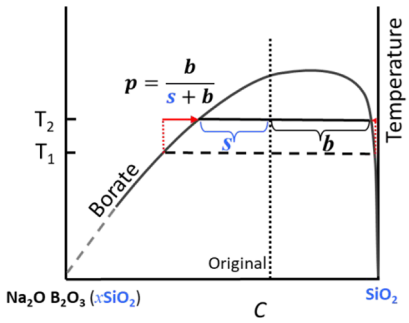

Figure 8. Schematic illustration of the two-step heat treatment in the G2 glass (the Al_2O_3 component is omitted). The glass with the original composition is allowed to phase separate at T_1 and then is elevated to T_2 in the second step to yield a new equilibrium following the red arrows. s and b express the constituents of the SiO_2-rich phase and borate-rich phase by $s = C_{original} - C_b$ and $b = C_s - C_{original}$, where $C_{original}$, C_b, and C_s are the concentrations of original glass, the borate-rich phase, and the SiO_2-rich phase, respectively. p is the fraction of the borate-rich phase in the phase separated glass, which contributes to the porosity of porous silica.

Figure 6(B) allowed us to draw detailed information on the growth in G2 glass at 600 °C. First, the data by the one-step process nearly obeyed eq 16 even without modification by eq 15. This suggests that the first stage of phase separation may be completed quickly at 600 °C. Second, the glasses by the two-step process deviated from the line of $d \propto t^{1/3}$ at 5 h. The initial scatterings provided information on the process for reaching the new equilibrium at 600 °C.

The parameter of A was estimated to be 78×10^3 nm^3 h^{-1} from the data of the glasses by the one-step process at 600 °C by disregarding the first stage of phase separation. When three relations of $t' = t - 2.5$, $t' = t - 1$, and $t' = t + 2.5$ were applied for the first steps at 520, 540, and 560 °C, respectively, the data by the second steps were strikingly fit into a straight line in Figure 6B (not shown). Furthermore, by assuming the periodic distances attained in the first steps for d_1, t_1 in eq 15 was estimated to be about 3.5, 2.5, and 1 h for the dissolution at 600 °C for the first steps at 520, 540, and 560 °C, respectively. Since the fraction of SiO_2-rich phase decreased with increasing temperature in the first step and then decreased toward the same value during the second step at 600 °C, such a tendency in t_1 seems reasonable.

As for parameter A, in addition to the interfacial energy (γ), it varies with the concentration (c) and mobility (B) of SiO_2 (eq 13). In the borate-rich phase with a fluidic nature, SiO_2 is broken by forming nonbridging oxygens of Si−O$^-$Na$^+$, the bonds of Si−O−B, and a small fraction of Si−O−Al. With an increase of temperature, parameter A should increase with both c and B.

As for the optical application, d should be as narrow as possible in order to lower the light scattering from the microstructure. On the basis of eqs 15 and 16, if t is adjusted to minimize t' in the second step; the average periodic distance may be further narrowed. The skeletons, however, can be kept close to those of the first two steps. On the other hand, to attain an antireflection of ∼0.5% in reflectivity, the porosity needed to be raised to ∼60%.[12] The equilibrium temperature in the second step should be elevated to ∼600 °C for the glass compositions frequently used. In the G2 glass, the fraction of the borate-rich phase $[b/(s + b)]$ rose at the second steps, and the porosities

https://doi.org/10.1021/acsphyschemau.4c00060
ACS Phys. Chem Au 2024, 4, 696−706

reached ∼62%. Consequently, as seen in Figure 7, the two-step processes provided the new region of spinodal structure, which had higher values of f.

In addition to the stereological analysis, the average periodic distances (d) were available from the data by ImageJ analysis in Figure 7 via the relation of $d = w/[1.2 \times (1 - \nu)]$ (w: width of skeletons, ν: porosity, f: fraction of dark area and $\nu = f + 20\%$),[53] and they ranged from 57 to 93 nm.

In the antireflective coating on the silica substrate, the reflectivity at the interface was reduced to the level of 0.07%.[13] If the porosity is raised to ∼70% with a favorable mechanical strength in the future, the refractive index becomes as low as 1.115 and the antireflection with a reflectivity less than 0.4% can be realized. This coating may find application in systems using a high-energy beam of light. In addition, a bulk of porous silica was attained from the G3 glass for the antifogging properties, where the porosity and the average periodic distance were found to be 59% and 41 nm, respectively.[14]

6. CONCLUSIONS

Both the introduction of Al_2O_3 and the two-step process were effective in exploring the region of spinodal structure in the $Na_2O-B_2O_3-SiO_2$ system, where the periodic distances between skeletons were reduced and the porosities increased to the high degree of ∼60%.

In relation to the theoretic treatments, the role of A_2O_3 in the phase separation was ascribed to the lowered interface energy between the two phases, which facilitated the formation of a spinodal structure having small periodic distances and made easy the establishment of durable silica skeletons against etching. In the two-step process, the growth during the later step could be well expressed by the basic relation of $d^3 = At'$, where t' was the heat-treatment time modified by incorporating both the initial dissolution process at the elevated temperature and the periodic distance attained at the first step.

■ ASSOCIATED CONTENT

Data Availability Statement

Data underlying the results presented in this paper are not publicly available at this time but may be obtained from the author by reasonable request and proper approval.

Supporting Information

The Supporting Information is available free of charge at https://pubs.acs.org/doi/10.1021/acsphyschemau.4c00060.

Stereological analysis of micrographs and ImageJ analysis of micrographs (PDF)

■ AUTHOR INFORMATION

Corresponding Author

Zuyi Zhang − *Nanomatereials Development Dept. 11, Nanomaterials R&D Center, R&D Headquarters, Canon Inc., Tokyo 146-8501, Japan;* Present Address: Core Technology Development Headquarters, Canon Inc., 30-2, Shimomaruko 3-chome, Ohta-ku, Tokyo 146-8501, Japan; orcid.org/0000-0002-2955-8337; Email: zhang.zuyi@mail.canon

Complete contact information is available at: https://pubs.acs.org/10.1021/acsphyschemau.4c00060

Notes

The author declares no competing financial interest.

■ ACKNOWLEDGMENTS

This study was performed in a project in R&D, Canon, with support from Operation Division from 2009 to 2013. The author thanks Dr. K. Takashima for his contribution in the preparation of porous samples, the SEM observation, and the analysis by ImageJ. The author is grateful to Mr. S. Kuroyanagi of Akagawa Glass Company for the measurements of Tg and for discussion with him. The author thanks Dr. T. Akai for the advice on the nature of phase separated glasses.

■ REFERENCES

(1) Nordberg, M. E. Properties of some Vycor-Brand Glasses. *J. Am. Ceram. Soc.* **1944**, *27*, 299−304.
(2) Mazurin, O. V.; Porai-Koshits, E. A. *Phase separation in glass*; North-Holland: Amsterdam, 1984.
(3) Varshneya, A. K. *Fundamentals of Inorganic Glass*; Academic Press: New York, 1994.
(4) Nakanishi, K.; Soga, N. Phase Separation in Gelling Silica−Organic Polymer Solution: Systems Containing Poly (sodium styrenesulfonate). *J. Am. Ceram. Soc.* **1991**, *74*, 2518−2530.
(5) Haller, W.; Blackburn, D. H.; Wagstaff, F. L.; Charles, R. J. Metastable Immiscibility Surface in the System $Na_2O-B_2O_3-SiO_2$. *J. Am. Ceram. Soc.* **1970**, *53*, 34−39.
(6) Kingery, W. D.; Bowen, H. K.; Uhlmann, D. R. *Introduction to Ceramics*; Wiley: New York, 1976.
(7) Flory, P. J. *Principles of Polymer Chemistry*. Cornell University Press: Ithaca, 1953.
(8) Nakanishi, K. Functional Porous Materials via Sol-Gel with Phase Separation. *J. Ceram. Soc. Jpn.* **2007**, *115*, 169−175.
(9) Nakanishi, K. Sol−Gel Process of Oxides Accompanied by Phase Separation. *Bull. Chem. Soc. Jpn.* **2006**, *79*, 673−691.
(10) Eguchi, K. Utilization of High Silica Porous Glass. *J. Jpn. Inst. Met. Mater.* **1984**, *23*, 989−995.
(11) Nakanishi, K.; Tanaka, N. Sol−Gel with Phase Separation. Hierarchically Porous Materials Optimized for High-Performance Liquid Chromatography Separations. *Acc. Chem. Res.* **2007**, *40*, 863−873.
(12) Zhang, Z. antireflective film of porous silica. *J. Opt. Soc. Am. A* **2022**, *39*, 1172−1178.
(13) Zhang, Z. Dust proof properties of spinodal porous surfaces. *J. Opt. Soc. Am. A* **2022**, *39*, 866−872.
(14) Zhang, Z. Antifogging properties of spinodal porous structures for optical application. *Langmuir* **2022**, *38*, 7448−7454.
(15) Saiki, K.; Sakida, S.; Benino, Y.; Nanba, T. Phase separation of borosilicate glass containing sulfur. *J. Ceram. Soc., Jpn.* **2010**, *118*, 603−607.
(16) Kikuta, H. New Technologies for Reduction of Light Reflection. *Jpn. J. Opt.* **2011**, *40*, 2−10.
(17) Okuno, T. The Development of Subwavelength Structure Coating and Its Application to Camera Lenses. *Jpn. J. Opt.* **2011**, *40*, 11−16.
(18) Murata, G. Development of Super-High Performance antireflective Coatings Using Fluoride Nanoparticles. *Jpn. J. Opt.* **2011**, *40*, 17−23.
(19) Ogawa, S.; Nakamura, J. Fractal and spinodal-decomposed turbidities of nanoporous glass: fluctuation picture in turbid and transparent Vycor. *J. Opt. Soc. Am. A* **2017**, *34*, 449−463.
(20) When the average periodic distance is small compared to the wavelength of light, Rayleigh scattering from an inhomogeneous coating is expressed by a relation of $I \sim \langle \eta^2 \rangle \{8\pi^3\rho^3/[(1 + 4\pi^2\rho^2)^2\lambda^4]\}d^3l$, which is derived from Eq. 12 in Ref 19. Here, I is the scattering intensity per area at the wavelength of λ. η is dielectric constant, and $\langle \eta^2 \rangle$ is average value of η^2; l, d and ρ are the thickness of inhomogeneous coating, the average periodic distance and a ratio characteristic of the

periodicity of structure (ζ/λm, a correlation length/a wavelength of the density fluctuation), respectively.
(21) Charles, R. J. Phase Separation in Borosilicate Glasses. *J. Am. Ceram. Soc.* **1964**, *47*, 559−563.
(22) In Fig. 1, two symmetric curves are employed for the compositional dependences of free energy between the concentrations of two phases, since there is no rigorous information for possible asymmetry except for the immiscibility gap (ref 3.). Following ref 6., horizontal lines indicate the respective levels of free energy qualitatively for ΔG by phase separation at T_1, a relative change between two temperatures under equilibrium conditions (black lines) and another change with the compositions inheriting from the equilibrium at T_1 (pink line).
(23) Takamori, T.; Tomozawa, M. Viscosity and Microstructure of Phase-Separated Borosilicate Glasses. *J. Am. Ceram. Soc.* **1979**, *62*, 373−377.
(24) Tanaka, H. Viscoelastic phase separation. *J. Phys.: Condens. Matter* **2000**, *12*, R207.
(25) Cahn, J. W.; Hilliard, J. E. Free Energy of a Nonuniform System. I. Interfacial Free Energy. *J. Chem. Phys.* **1958**, *28*, 258−267.
(26) Cahn, J. W. On spinodal Decomposition. *Acta Metall.* **1961**, *9*, 795−801.
(27) Tanaka, H.; Yazawa, T.; Eguchi, K. Sintering Temperature of Porous Glass and Transition Temperature of High Silica Glass. *J. Ceram. Soc. Jpn.* **1986**, *94*, 564−570.
(28) In literature, both terminologies of etching and leaching are used for the spinodal porous silica. Here, etching is preferred because the temperature was elevated to 90°C to avoid colloidal silica from the borate-rich phase (also see Ref 14).
(29) EGUCHI, K.; UETUKI, T.; TARUMI, S. Swell or Shrinkage of Borosilicate Glass during Acid Leaching. *J. Ceram. Soc. Jpn.* **1979**, *87*, 558−564.
(30) Hood, H. P.; Morberg, M. E. *Treated Borosilicate Glass*, 1938 USP 2106744.
(31) Tomozawa, M.; Sridharan, S.; Takamori, T. Origin of Viscosity Increase of Phase-Separated Borosilicate glasses. *J. Am. Ceram. Soc.* **1992**, *75*, 3103−3110.
(32) Tanaka, H.; Yazawa, T.; Eguchi, K.; Nagasawa, H.; Matsuda, N.; Einishi, T. Precipitation of colloidal silica and pore size distribution in high silica porous glass. *J. Non-Cryst. Solids* **1984**, *65*, 301−309.
(33) Burnett, D. G.; Douglas, R. W. Liquid−liquid phase separation in the soda−lime−silica system. *Phys. Chem. Glasses* **1970**, *11*, 125−135.
(34) McMillan, P. W.; Matthews, C. E. Microporous glasses for reverse osmosis. *J. Mater. Sci.* **1976**, *11*, 1187−1199.
(35) Craievich, A. F.; Zanotto, E. E.; James, P. F. Kinetics of sub-liquidus phase separation in silicate and borate glasses. *A review. Bull. Mineral* **1983**, *106*, 169−184.
(36) Xianping, F.; Quanqing, C. Study of phase separation in Na2O-B2O3-SiO2 glasses by tem and optical diffraction. *J. Non-Cryst. Solids* **1989**, *112*, 232−237.
(37) Vasilevskaya, T. N.; Andreev, N. S. Experimental Small-Angle X-Ray Scattering Investigation of Initial Stages of the spinodal Decomposition in Model Sodium Silicate Glasses. *Phys. Solid State* **2011**, *53*, 2250−2262.
(38) Dalmas, D.; Lelarge, A.; Vandembroucq, D. Crack Propagation through Phase-Separated Glasses: Effect of the Characteristic Size of Disorder. *Phys. Rev. Lett.* **2008**, *101*, No. 255501.
(39) Wheaton, B. R.; Clare, A. G. Evaluation of phase separation in glasses with the use of atomic force microscopy. *J. Non-Cryst. Solids* **2007**, *353*, 4767−4778.
(40) Feng, W.; Bonamy, D.; Célarié, F.; Fossati, P. C. M.; Gossé, S.; Houizot, P.; Rountree, C. Stress Corrosion Cracking in Amorphous Phase Separated Oxide Glasses: A Holistic Review of Their Structures, Physical, Mechanical and Fracture Properties. *Corros. Mater. Degrad.* **2021**, *2*, 412−466.
(41) Porter, D. A.; Eastering, K. E. *Phase Transformation in Metals and Alloys*; Chapman & Hall: Boca Raton, 1992.
(42) Lifshitz, I. M.; Slyozov, V. V. The kinetics of precipitation from supersaturated solid solutions. *J. Phys. Chem. Solids* **1961**, *19*, 35−50.
(43) Wagner, C. Theorie der Alterung von Niederschlagen durch Umlosen (Ostwald-Reifung). *Z. Elektrochem* **1961**, *65*, 581−591.
(44) Haller, W. Rearrangement Kinetics of the Liquid−Liquid Immiscible Microphases in Alkali Borosilicate Melts. *J. Chem. Phys.* **1965**, *42*, 686−693.
(45) Adamson, A. W. *Physical Chemistry of Surfaces*; Interscience Publishers: New York, 1967.
(46) Davies, J. T.; Rideal, E. K. *Interfacial Phenomena*; Academic Press: New York, 1963.
(47) As for the thermodynamic process with a change in temperature from T_1 to T_2, two hypotheses were taken into consideration. First, the average width of SiO_2 skeletons decreases without changing the density in number of the skeletons. Second, the density of skeletons in number decreases without changing the average width. In this study, the first one was chosen for the later discussion tentatively.
(48) Eguchi, K.; Tasaka, K.; Tarumi, S. Effect of Composition on the Heat-treatment Time for Phase-separating Borosilicate Glasses and the Time for Leaching the Separated Glasses. *J. Ceram. Soc. Jpn.* **1969**, *77*, 301−309.
(49) As the supporting information, the glass samples of G3 and G4 phase separated at 600°C were also investigated by TMA. The transition temperatures remained essentially unchanged after the phase separation. Instead of yield points below 600°C, there were plateaus of length with the temperature ranges of 610−630°C and 625−675°C for G3 and G4 glasses, respectively. This implies the solidification of structure due to the interconnected SiO_2-rich phase (see Discussion).
(50) Smedskjaer, M.; Youngman, R.; Mauro, J. Principle of Pyrex glass chemistry: structure−property relationships. *Appl. Phys. A: Mater. Sci. Process.* **2014**, *116*, 491−504.
(51) Minot, M. J. Single-layer, gradient refractive index antireflection films effective from 0.35 to 2.5 μ,. *J. Opt. Soc. Am.* **1976**, *66*, 515−519.
(52) Schneider, C. A.; Rasband, W. S.; Eliceiri, K. W. NIH Image to ImageJ: 25 years of image analysis. *Nat. Methods* **2012**, *9*, 671−675.
(53) The practical porosities of porous silica (ν) could be calculated from their reflections in visible region by using Lorentz-Lorenz equation and assuming n_0=1.420 for silica skeletons. The calculation method was described in Ref 12. We confirmed that, the fractions of dark area (f) by ImageJ were 20% lower than the porosities.
(54) Minamiyama, S.; Daiko, Y.; Mineshige, A.; Kobune, M.; Yazawa, T. spinodal-type phase separation and proton conductivity of Al_2O_3-doped porous glasses. *J. Ceram. Soc. Jpn.* **2010**, *118*, 1131−1134.
(55) Du, W. F.; Kuraoka, K.; Akai, T.; Yazawa, T. Study of Al_2O_3 effect on structural change and phase separation in $Na_2O-B_2O_3-SiO_2$ glass by NMR. *J. Mater. Sci.* **2000**, *35*, 4865−4871.
(56) MACDOWELL, J. F.; BEALL, G. H. Immiscibility and Crystallization in A12O3-SiO2 Glasses. *J. Am. Ceram. Soc.* **1969**, *52*, 17−25.
(57) Kwinda, T. I.; Enke, D.; Koppka, S. Effect of TiO_2 on microphase development during phase separation and crystallization in $Na_2O-B_2O_3-SiO_2$ glass system. *J. Am. Ceram. Soc.* **2022**, *105*, 3261−3278.
(58) On the assumption of eq 3, the concentration of SiO_2 in the borate-rich phase changes with the curvature radius of the interface ($\bar{r}$), and $C_b \sim S_0 \exp(2\gamma V_m/RT\bar{r})$. Practically, however, the immiscibility gap ($C_b \sim C_s$) in literature was determined roughly based on the disappearance of transparency due to the phase separation, and C_b is generally regarded as S_0. If a value of 285 mNm^{-1} of γ for SiO_2 melt at 1400°C (Fukumi, K.; Kitamura, N.; Hirano, T.; Kozuka, H.; Nishii, J. *New Glass* 2009, *20*, 3−7) was applied for the interface at 600°C, the term of $\exp(2\gamma V_m/RT\bar{r})$ ranges from 1 − 0.045 to 1 in correspondence to a change in $\bar{r}$ from −50 nm to ∞. This term is expected to be closer to 1 in G2 glass due to the reduced interfacial energy. Here, the change in the fraction of borate-rich phase (porosity) with temperature was explained only from the change in S_0 for convenience (Fig. 8).

https://doi.org/10.1021/acsphyschemau.4c00060
ACS Phys. Chem Au 2024, 4, 696−706